

Spin dynamics of the E_8 particles

Xiao Wang,¹ Konrad Puzniak,^{2,3} Karin Schmalzl,⁴ C. Balz,⁵ M. Matsuda,⁶ Akira Okutani,⁷ M. Hagiwara,⁷ Jie Ma,^{1,8,9,*} Jianda Wu,^{1,8,10,†} and Bella Lake^{2,3,‡}

¹*Tsung-Dao Lee Institute, Shanghai Jiao Tong University, Shanghai, 201210, China*

²*Helmholtz-Zentrum Berlin für Materialien und Energie GmbH, Hahn-Meitner Platz 1, D-14109 Berlin, Germany*

³*Institut für Festkörperphysik, Technische Universität Berlin, Hardenbergstraße 36, D-10623 Berlin, Germany*

⁴*Jülich Centre for Neutron Science JCNS, Forschungszentrum Jülich GmbH, Outstation at ILL, 38042 Grenoble, France*

⁵*ISIS Neutron and Muon Source, STFC Rutherford Appleton Laboratory, Didcot OX11 0QX, United Kingdom*

⁶*Neutron Scattering Division, Oak Ridge National Laboratory, Oak Ridge, Tennessee 37831, USA*

⁷*Center for Advanced High Magnetic Field Science, Graduate School of Science, Osaka University, Osaka 560-0043, Japan*

⁸*School of Physics & Astronomy, Shanghai Jiao Tong University, Shanghai, 200240, China*

⁹*Collaborative Innovation Center of Advanced Microstructures, Nanjing 210093, China*

¹⁰*Shanghai Branch, Hefei National Laboratory, Shanghai 201315, China*

In this article, we report on inelastic neutron scattering measurements on a quasi-1D antiferromagnet $\text{BaCo}_2\text{V}_2\text{O}_8$ under a transverse magnetic field applied along the (0,1,0) direction. Combining results of inelastic neutron scattering experiments, analytical analysis, and numerical simulations, we precisely studied the E_8 excitations appearing in the whole Brillouin zone at $B_c^{1D} \approx 4.7$ T. The energy scan at $Q = (0, 0, 2)$ reveals a match between the data and the theoretical prediction of energies of multiple E_8 excitations. Furthermore, dispersions of the lightest three E_8 particles have been clearly observed, confirming the existence of the E_8 particles in $\text{BaCo}_2\text{V}_2\text{O}_8$. Our results lay down a concrete ground to systematically study the physics of the exotic E_8 particles.

Unlike the classical phase transition driven by thermal fluctuations, the quantum phase transition arises at zero temperature when the system is tuned by a non-thermal parameter [1]. For a continuous quantum phase transition, novel physics with higher symmetry may emerge at the quantum critical point (QCP), classified by a set of critical exponents manifested into scaling form [1]. Moreover, when the system is driven away from the QCP with a relevant perturbation, exotic physics may further emerge due to the strong renormalization of the almost infinite low-lying excitations, which is “emergence of emergence” [2–4].

One such paradigmatic model is the transverse-field Ising chain (TFIC) [1, 5]. When an Ising chain is tuned to its QCP by a magnetic field applied transverse to its Ising anisotropy, a central charge 1/2 conformal field theory emerges with corresponding scaling exponents falling into the class of Ising universality see Fig. 1 [5, 6]. Surprisingly, when it is further perturbed by a longitudinal field parallel to the Ising direction, the quantum E_8 integrable model emerges - a massive relativistic quantum field theory containing eight massive E_8 particles whose relative masses have precise values as listed in the first row of Table I. The physics of the model is described by scattering of the E_8 particles, which is characterized by the maximal exceptional Lie E_8 algebra [2, 7–10].

For the experimental realization of the exotic E_8 physics, two conditions need to be satisfied: accessing the Ising universality and the presence of a small perturbation field along the Ising direction. An early inelastic neutron scattering (INS) experiment on the ferromagnetic chain compound CoNb_2O_6 provided evidence of the existence of the lightest two particles: the ratio of the energies of the lowest two peaks echos the Golden ratio of the two lightest E_8 particles’ masses [11]. However, there is an apparent deviation in the spectrum con-

tinuum region between the recent THz experiment on the material [9] and the analytical result [10], which implies more efforts [12, 13] are needed for confirming the existence of the E_8 physics in the material CoNb_2O_6 .

Recently, the quasi-1D Heisenberg-Ising antiferromagnetic (AFM) material $\text{BaCo}_2\text{V}_2\text{O}_8$ (a member of a family of materials with formula $AM_2V_2O_8$ in which: $A = \text{Sr, Ba}$, and the magnetic ions are $M = \text{Cu, Ni, Co, Mn}$), has attracted the attention of several experimental studies [14, 15]. When the materials are tuned by a transverse magnetic field, quantum criticality with Ising universality is observed [8]. Then the E_8 excitations with zero transfer momentum have been sought at low temperatures where the interchain coupling and long-range magnetic order provide the longitudinal field [8, 9]. These E_8 excitations are measured by inelastic neutron scattering [8] (in this case all the E_8 particles were found) and terahertz spectroscopy [9] (in the latter case the excitations up to the fifth E_8 particles were found) and compared successfully to theory.

However, all these measurements were confined to *only* the AFM zone center where the precise E_8 masses have already been calculated. Furthermore, other peaks due to combinations of the E_8 particles and zone folding were also observed, which, while fully explainable, resulted in many overlapping excitations decreasing the certainty of the results. Considering that the E_8 model is a massive relativistic quantum field theory, a full investigation of the *relativistic dispersion* of the E_8 particles in the whole Brillouin zone is necessary for a complete realization of the E_8 physics in the material $\text{BaCo}_2\text{V}_2\text{O}_8$.

In this work, we combine and compare experimental, analytical, and numerical approaches for the dispersion of the lightest three branches of excitations and unambiguously

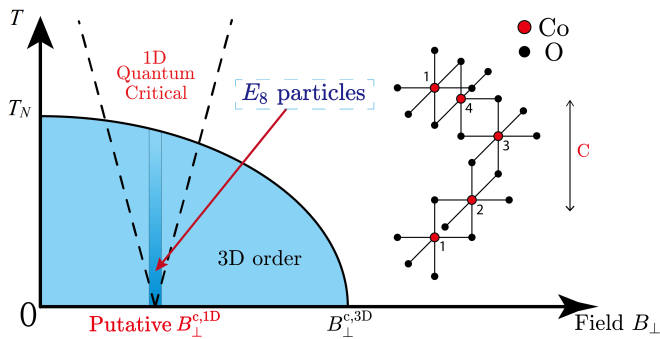


FIG. 1: Schematic phase diagram of $\text{BaCo}_2\text{V}_2\text{O}_8$ in a transverse magnetic field, light blue indicates the AFM order phase while the deep blue area covers the location of emergent exotic E_8 particles around the putative 1D QCP. The inset shows one of the CoO_6 screw chains.

demonstrate the existence of the exotic E_8 particles in the AFM material $\text{BaCo}_2\text{V}_2\text{O}_8$. $\text{BaCo}_2\text{V}_2\text{O}_8$ crystallizes in tetragonal symmetry (space group $I4_1/acd$ No. 142) with the lattice parameters: $a = b = 12.40 \text{ \AA}$ and $c = 8.375 \text{ \AA}$ [15]. The magnetic Co^{2+} ions have effective spin of $S = \frac{1}{2}$ and are arranged in edge-sharing CoO_6 octahedra forming 4-fold screw chains running along the c -axis (see inset of Fig. 1). There are four screw chains per unit cell, two of which rotate clockwise while the other two rotate anticlockwise [16]. The Co^{2+} ions are coupled by strong AFM interactions within the screw chains which have partial Ising (XXZ) anisotropy favouring spin directions parallel to the c -axis. In the absence of an external magnetic field, $\text{BaCo}_2\text{V}_2\text{O}_8$ develops a long-range magnetic Néel order below $T_N = 5.5 \text{ K}$ due to weak interchain coupling, where neighboring spins are aligned antiferromagnetically along the screw chains and ferromagnetically (antiferromagnetically) between chains along the a (b) direction respectively. The spins point almost parallel to the c -axis.

Under an external transverse magnetic field applied perpendicular to the spin direction (e.g. parallel to the b -axis), $\text{BaCo}_2\text{V}_2\text{O}_8$ undergoes a three-dimensional (3D) quantum phase transition at $\mu_0 H_{\perp}^{c,3D} \approx 10.3 \text{ T}$ (Fig. 1) that was identified, by a combination of field theory, numerical analysis, and neutron scattering experiments, as a spin-flop transition from the c to a directions [14]. This transition originates from the complex g -factor of $\text{BaCo}_2\text{V}_2\text{O}_8$. A one-dimensional (1D) quantum phase transition was also discovered at the lower transverse magnetic field of $\mu_0 H_{\perp}^{c,1D} = 4.7 \text{ T}$ [8, 17]. This transition lies hidden within the dome of the 3D magnetic order (see Fig. 1) which provides the (staggered) longitudinal magnetic field required for the emergence of the E_8 quantum particles.

The aim of this paper is to investigate $\text{BaCo}_2\text{V}_2\text{O}_8$ at its putative critical transverse field $\mu_0 H_{\perp}^{c,1D} \approx 4.7 \text{ T}$ [8] by combining an inelastic neutron scattering study of the dispersion of E_8 particles with a theoretical analysis based on the infinite time-evolving block decimation (iTEBD) technique [18]. The

plan of this paper is as follows: firstly we describe our experimental and theoretical approaches, then the neutron measurements of the dispersion of E_8 particles are presented and compared to the numerical simulations based on the iTEBD technique. Excellent agreement is achieved as a function of wavevector and energy for the lowest three E_8 particles.

Two large, high-quality single crystals of $\text{BaCo}_2\text{V}_2\text{O}_8$ were grown using the floating-zone technique at Osaka University, Japan, and at the Core Lab for Quantum Materials, Helmholtz Zentrum Berlin für Materialien und Energie (HZB), Germany. Inelastic neutron scattering was performed to measure the magnetic excitations on the cold neutron multichopper spectrometer, LET (at the ISIS Facility, Rutherford Appleton Laboratory, UK) using the HZB crystal (mass 4.13 g) [19]. INS experiments were also performed on the cold neutron triple-axis spectrometer, IN12 from the Forschungszentrum Jülich Collaborating Research Group (FZJ-CRG) installed at Institut Laue Langevin (ILL) France, using the Osaka crystal (mass 3.66 g).

For the LET experiment, the single crystal was aligned in the $(0, K, L)$ horizontal scattering plane and a vertical field cryomagnet was used to apply a constant magnetic field of $B = 4.7 \text{ T}$ along the a -axis to reach the 1D QCP. These measurements were carried out at $T = 0.3 \text{ K}$ using a ^3He -insert. This temperature is well below the Néel temperature ($T_N = 5.5 \text{ K}$) ensuring the presence of the effective longitudinal perturbing field necessary to stabilize E_8 physics. Using repetition rate multiplication and the chopper frequencies 280/140 Hz, incident neutron energies of $E_i = 22.69, 13.21, 8.51, 6.00, 4.42, 3.42, 2.70 \text{ meV}$ were achieved with corresponding elastic energy resolutions of $\Delta E = 0.91, 0.41, 0.22, 0.14, 0.094, 0.065, 0.048 \text{ meV}$. The INS data were processed using the MANTID and HORACE software packages and converted to absolute units. The spectrum for the incident energy of 6 meV is displayed in Fig. 2 as a function of energy and wavevector transfer along the chain direction, $(0, 0, L)$.

For the IN12 experiment, the crystal was aligned with the a - and c -axes within the horizontal instrumental scattering plane and a vertical DC magnetic field of 4.7 T was applied parallel to the b -axis. A fixed final wavevector of $k_f = 1.15 \text{ \AA}^{-1}$ was used, giving an energy resolution of $\Delta E \approx 0.114 \text{ meV}$ and wavevector resolution of $\approx 0.067 \text{ r.l.u.}$ A Beryllium filter was used to suppress higher-order wavelengths and spurious scattering. A series of energy scans at constant wavevector in the range from $\mathbf{Q} = (0, 0, 1.5)$ to $(0, 0, 2.5)$ were performed over the energy range from $E = 0.5 \text{ meV}$ with steps of at least 0.05 meV. Constant-energy scans were also performed within this range. These measurements took place at a temperature of $T = 1.50 \text{ K} (\ll T_N)$. The constant-energy and constant-wavevector scans are combined together to make the energy-wavevector map in Fig. 3 (c).

When applying a transverse field along $(0, 1, 0)$ direction, the effective Hamiltonian for $\text{BaCo}_2\text{V}_2\text{O}_8$ is described by a

TABLE I: Predicted ratios of the energies of the single E_8 particle (first row) and the multi-particle (second row) excitations along with their expected values in $\text{BaCo}_2\text{V}_2\text{O}_8$ (third row). The experimental excitation energies at various wavevectors from LET and IN12 are then listed along with the values obtained from iTEBD.

Single	m_1	m_2	m_3	m_4	m_5	m_6	m_7						
Multi	$2m_1$			m_1+m_2	m_1+m_3	$3m_1$	$2m_2$						
Theoretical ratio m_i/m_1	1	1.618	1.989	2	2.405	2.618	2.956	2.989	3	3.218	3.236	3.891	
$\text{BaCo}_2\text{V}_2\text{O}_8$ theory [meV]	1.26	2.04	2.50	2.52	3.03	3.30	3.72	3.73	3.75	4.05	4.08	4.90	
LET [meV]	(0,0,2)	1.28	2.04	2.52	2.58	3.04	3.30	-	-	-	-	-	
IN12 [meV]	(0,0,2)	1.26	2.05	2.49	-	-	-	-	-	-	-	-	
iTEBD [meV]	(0,0,2)	1.26	2.06	2.50	2.52	3.06	3.32	3.64	3.70	3.78	4.04	4.10	4.84

1D spin-1/2 Heisenberg-Ising model [8, 9, 17, 20, 21]:

$$\begin{aligned}
\mathcal{H} &= H_{XXZ} + H_t + H_s \\
H_{XXZ} &= J \sum_n [S_n^z S_{n+1}^z + \epsilon (S_n^x S_{n+1}^x + S_n^y S_{n+1}^y)] \\
H_t &= -\mu_B g_{yy} H \sum_n [S_n^y + h_x (-1)^n S_n^x \\
&\quad + h_z \cos(\pi \frac{2n-1}{4}) S_n^z] \\
H_s &= -\mu_B H' \sum_n (-1)^n S_n^z
\end{aligned} \tag{1}$$

where $S_n^\alpha = \frac{1}{2} \sigma_n^\alpha$ ($\alpha = x, y, z$) are spin-1/2 operators at site n with Pauli matrices σ^α . $J = 5.8$ meV, $\epsilon = 0.46$, $h_x(z) = 0.4(0.14)$, $g_{yy} = 2.75$. The applied transverse field is set $\mu_0 H = 4.7$ T, which is the critical field of the putative 1D QCP [8, 21]. The effective staggered longitudinal field $\mu_B H' = 0.018J$ comes from a mean-field treatment of the inter-chain coupling in the 3D ordering region below T_N [8, 14]. H_s provides a necessary relevant perturbation for realizing the quantum E_8 physics [8]. Focusing on the parameter region around the putative 1D QCP, in the scaling limit, the effective Hamiltonian of the spin chain becomes [7, 8, 10]

$$\mathcal{H}_{E_8} = \mathcal{H}_{c=1/2} + h \int dx \sigma(x). \tag{2}$$

$\mathcal{H}_{c=1/2}$ is the Hamiltonian for a central charge 1/2 conformal field theory, which describes the quantum critical physics of the TFIC. h and $\sigma(x)$ corresponding to the scaling limits of $\mu_B H'$ and σ_j^z are the strengths of the perturbation field and the relevant primary field, respectively.

To determine the dispersion of E_8 particles and compare with the spectrum measured by INS, we calculate the spin dynamic structure factor (DSF) in the field theory frame, $D^{\alpha\alpha}(\omega, q) = \sum_{n=1}^{\infty} \frac{(2\pi)^2}{\prod_{a_i=1}^8 n_{a_i}!} \int_{-\infty}^{\infty} \prod_{j=1}^n \frac{d\theta_j}{2\pi} |\langle 0 | \sigma^\alpha | A_{a_1}(\theta_1) \dots A_{a_n}(\theta_n) \rangle|^2 \delta(\omega - \sum_{j=1}^n E_j) \delta(q - \sum_{j=1}^n P_j)$, where $\alpha = x, z$, and $a_i = 1 \dots 8$ are quasi-particles obtained from the quantum E_8

integrable theory [2, 7, 8, 10]. n_{a_i} is the number of particle a_i involved in the corresponding channel. $E_j = m_{a_j} \cosh \theta_j$ and $P_j = m_{a_j} \sinh \theta_j$ are the energy and momentum of particle a_j in terms of the rapidity θ . The two Dirac δ -functions reflect the energy and momentum conservation of the scattering. The DSF of $\sigma^{x,z}$ can be directly calculated from quantum E_8 integrable field theory [10], and the DSF of σ^y can be obtained from DSF of σ^z [22]. The analytical result for the dispersion of the lightest three E_8 particles is shown in Fig. 3(a). For a better comparison of the theoretical prediction from quantum E_8 field theory with the INS experimental result, two subtle issues are worth noting.

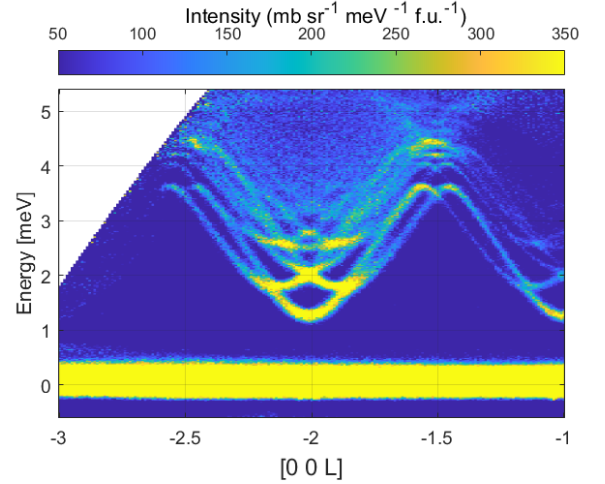


FIG. 2: Magnetic intensity of $\text{BaCo}_2\text{V}_2\text{O}_8$ measured in a transverse magnetic field of $\mu_0 H_{\perp}^{c,1D} = 4.7$ T at $T = 0.3$ K using the LET spectrometer. The data is displayed in absolute units as a function of wavevector $\mathbf{Q} = (0,0,L)$ and energy, for neutron incident energy $E_i = 6$ meV (integration range: $-1.0 \leq H \leq 1.0$ & $-2 \leq K \leq 2$).

1. In the above field theory frame calculation, the speed of light is set as $c = 1$. For the quantum E_8 model, as a massive relativistic quantum field theory, the dispersion of the E_8 particles follows the massive relativistic dispersion $E_i^2 = \Delta_i^2 + p_i^2 c^2$, where $\Delta_i = m_i c^2$ and $p_i = m_i c$ with the

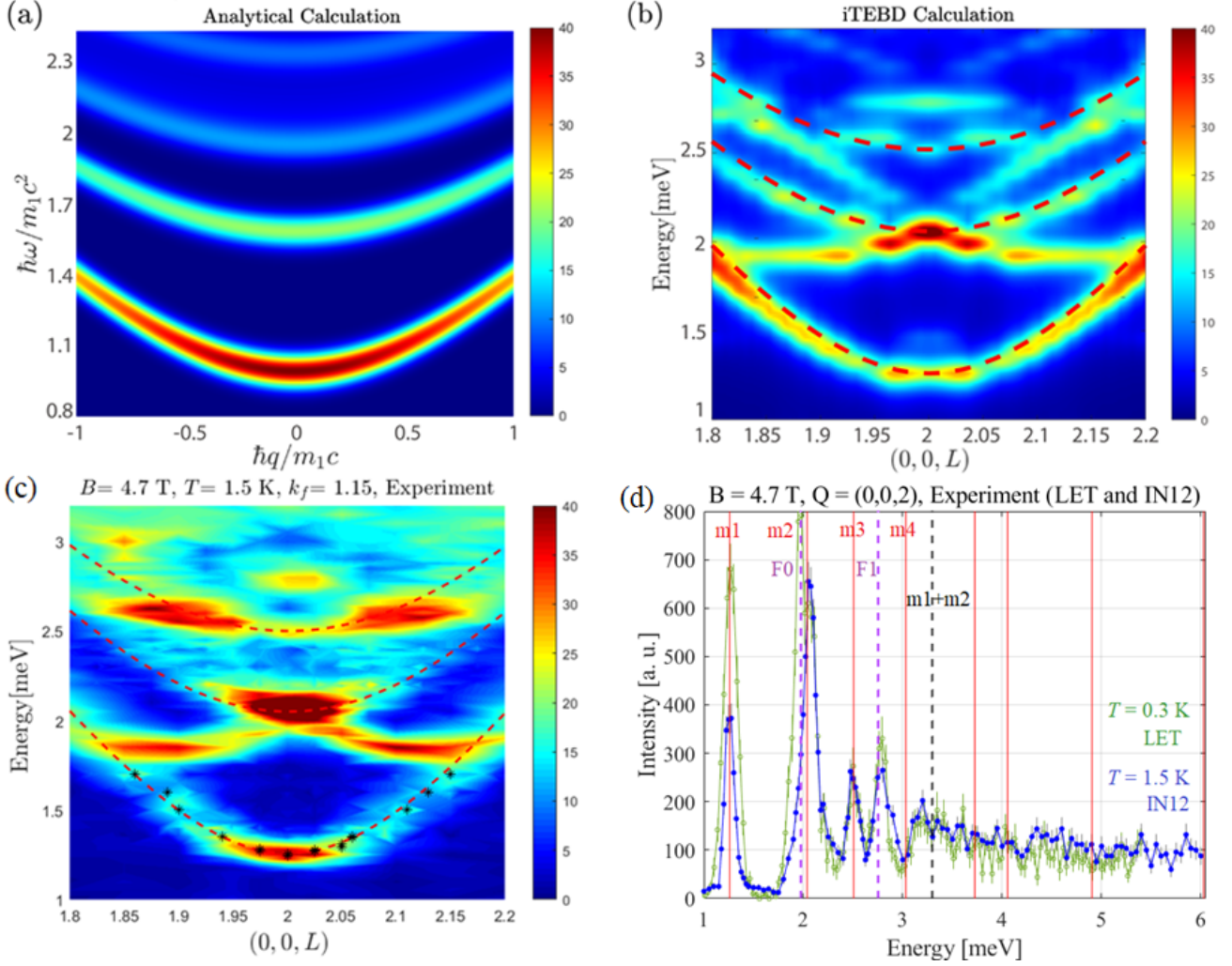


FIG. 3: (a) Analytical calculation of dispersion of three lightest E_8 particles. (b) Numerical simulation of dispersion using the iTEBD method, based on Eq. (9). The dashed lines illustrate dispersions of the three lightest E_8 particles given by Eq. (8). (c) Energy-wavevector map of the magnetic excitations constructed from constant-energy and constant-wavevector scans measured on the IN12 spectrometer at $B_c^{1D} = 4.7$ T and $T = 1.5$ K. The black symbols are the peak positions extracted from fitting the individual scans, whereas the dashed lines are fits to the dispersions to the lowest three E_8 particles using Eq. (8). (d) shows an energy scan measured at the wavevector $Q = (0,0,2)$ on LET and IN12, with the theoretically predicted energies of the first E_8 excitations indicated by the red solid lines. Identified peaks are labelled m_n (single E_8 excitations), $m_n + m_m$ (multi- E_8 excitations) and F_n (zone-folding peaks).

“rest mass” of the i^{th} E_8 particle m_i and the “speed of light” c . When coming to a real material which actually is a lattice discrete in space, we need to re-scale the dispersion of the E_8 particles with the proper energy scale and length (momentum) scale serving as IR cutoffs. The theoretically expected energy peak corresponding to the lightest E_8 particle m_1 can be estimated from $E_{m_1}^{\text{theory}} = C_{\text{lattice}} H^{18/15} \approx 1.2$ meV [23], where $C_{\text{lattice}} = 4.010 \dots$ is a modified constant for the lattice which originally comes from quantum E_8 field theory [24]. The value of $E_{m_1}^{\text{iTEBD}}$ matches the minimum gap $\Delta_1 = 1.26$ meV observed at the zone center (corresponding to zero transfer momentum), thus Δ_1 can naturally serve as IR cutoff of the energy scale for the experimental data. Since $\Delta_1 = m_1 c^2$ then we can pick up the corresponding IR momentum cutoff

$p_1 = m_1 c$. By applying these two IR cutoffs scales we arrive at

$$\frac{E_i^2}{\Delta_1^2} = \frac{\Delta_i^2}{\Delta_1^2} + \frac{p_i^2}{(\Delta_1/c)^2} = \frac{\Delta_i^2}{\Delta_1^2} + \left(\frac{\hbar(L-2)\pi/2d}{m_1 c} \right)^2, \quad (3)$$

where $p_i = \hbar(L-2)\pi/2d$ is the momentum transfer with respect to $Q = (0,0,2)$ and $d = 8.4192/4 = 2.105$ is the nearest neighbor distance between Co^{2+} ions projected onto the chain direction. We need to determine the value of c to obtain the IR cutoff for the momentum, whose value cannot be uniquely determined by the analytical theory but actually depends on the microscopic details of the material.

2. The four-fold periodicity of $\text{BaCo}_2\text{V}_2\text{O}_8$ leads to the sizable zone-folding effect of the experimental measurement,

which makes the E_8 particles' dispersion shadowed by additional spectra. Such an effect cannot be obtained from the field theory calculation, instead, we need to go back to the original effective lattice model. By comparing spectra obtained from the lattice model and the field theory, the E_8 particles' dispersion will be extracted.

To make these two subtle issues clear, we carry out iTEBD simulation for the effective Hamiltonian Eq. (6) with $J = 1$, $\epsilon = 0.47$, and critical field $\mu_B g_{yy} H = 0.15$ [8, 21],

$$D_{\text{lat}}^{\alpha\alpha}(\omega, q) = \frac{1}{N} \sum_{j,j'=1}^N \exp\{-iq(j-j')\} \times \int_{-\infty}^{\infty} dt \exp(i\omega t) \langle S_j^\alpha(t) S_{j'}^\alpha(0) \rangle, \quad (4)$$

with total number of lattice sites N ($N \rightarrow \infty$ in iTEBD), and spin-1/2 operators S^α , $\alpha = x, y, z$. The iTEBD simulation result is shown in Fig. 3 (b), where the value of the "speed of light" is found to be $c \approx (1.441 \pm 0.096) \times 10^3$ m/s and the zone-folding effect can be identified as well.

The procedure of the iTEBD calculation is as follows: 1. Generate a four-periodic ground state wave function of the effective Hamiltonian Eq. (6) with the parameters. The imaginary time-evolution is done with fifth-order Trotter-Suzuki decomposition [25], where the imaginary time slide is set as $d\tau = 0.01$. The convergence condition is chosen as the difference of the norm of singular values in the matrix product states being smaller than 10^{-12} . The truncated dimension is chosen as $\chi = 45$ [18, 26]. 2. Calculate the DSF [Eq. (9)] for S^x and S^z , while the DSF of S^y can be obtained from DSF of S^z by using $D^{yy}(\omega, q) = \omega^2 D^{zz}(\omega, q)/(4J^2)$ [22]. For calculating this DSF with iTEBD algorithm, we first do real time and space propagation in Heisenberg picture, then by using Fourier transformation we transform the obtained result into momentum and energy space to obtain the final spectrum. The real time evolution is done by a second order Trotter-Suzuki decomposition with $t = 200$, $dt = 0.02$ for obtaining a relatively high accurate result near the Brillouin zone center. 3. A zone-folding effect is necessary to consider when obtaining the final spectrum for comparison with INS experimental results.

The magnetic excitations of $\text{BaCo}_2\text{V}_2\text{O}_8$, measured using the LET time-of-flight spectrometer at $T = 0.3$ K and $\mu_0 H = \mu_0 H_\perp^{c,1D} (= 4.7$ T) with incident neutron energy of 6 meV, is shown in Fig. 2 as a function of energy and wavevector transfer along the chain direction. To complement this, Fig. 3 (c) shows the low-energy excitations built from the energy- and wavevector-scans measured at $T = 1.5$ K and $\mu_0 H = 4.7$ T on the IN12 spectrometer. An incredibly rich series of modes is found with complex dispersions and intensity modulations. First of all, the 4-fold screw-chain structure about the c -axis gives rise to four independent chain spectra shifted consecutively in wavevector along the chain by $\Delta L = 1$ r.l.u. Each individual spectrum is periodic over an interval of $\Delta L = 4$ r.l.u. due to the fact that there are four Co^{2+} ions along each chain per unit cell (because of the screw-chain

structure). Together these four spectra ensure that an antiferromagnetic zone center where the excitations are minimum is found at every integer value of L . At low energies, each spectrum is expected to consist of the E_8 -particles observed as sharp (resolution-limited) gapped modes. In addition, multi-particle excitations are expected, due to the simultaneous creation of two or more E_8 particles such as $m_1 + m_2$. These excitations form a continuum with a sharp lower boundary. Finally, zone-folding modes are expected which are a consequence of the screw chain structure of $\text{BaCo}_2\text{V}_2\text{O}_8$. Unlike the other excitations, these can be incommensurate with minima that do not always occur at integer values of L .

According to theory, the ratios of the energies of the eight E_8 -particles have precise values [27]. These values are given in the first row of Table I along with the expected values of the multiparticle excitations. The excitations were indeed observed previously at these energies at the antiferromagnetic zone centers (integer L -wavevectors) of $\text{BaCo}_2\text{V}_2\text{O}_8$ [8]. Here we reconfirm this observation using our higher resolution (but lower intensity) data. The energy scans through our LET and IN12 datasets are shown in Fig. 3(d). For both datasets, the first peak is observed at 1.26 meV. Multiplying the E_8 particle ratios by this value gives the theoretically expected peak positions for $\text{BaCo}_2\text{V}_2\text{O}_8$ (second row of Table I) which are also indicated by the solid vertical red lines in Fig. 3(d). The first three peaks in the LET and IN12 experimental data (at $m_1 = 1.26$, $m_2 = 2.04$, $m_3 = 2.52$ meV and at $m_1 = 1.26$, $m_2 = 2.05$, $m_3 = 2.49$ meV respectively) clearly lie at the expected positions of the first three E_8 peaks, (it should be noted that the multi-particle peak $2m_1$ coincides with m_3). It should be also noted that close to m_2 there is a zone-folding peak of 1.98 meV (indicated by F0). There exists also another zone-folding peak at 2.75 meV (indicated by F1). The fourth E_8 excitation at $m_4 = 3.04$ meV is very weak, while the feature at 3.30 meV is the lower boundary of the $m_1 + m_2$ multi-particle continuum. At higher energies, it is difficult to distinguish the E_8 peaks due to overlapping continua and zone-folding modes. The positions of peaks were found by fitting Gaussians. They are listed in Table I and are in agreement with the results of H. Zou *et al.* [8]. Because we collected high-precision data over a wide range of wavevectors rather than at just the antiferromagnetic zone centers, we now have the opportunity to observe the behavior of the E_8 -particles as well as the other excitations as a function of wavevector as well as energy. Returning to the energy-wavevector plots in Fig. 2 and 3(c), it is clear that the three lowest E_8 excitations actually form dispersive modes with parabolic curvature and a minimum at $\mathbf{Q} = (0,0,2)$. The zone-folding modes are now easily identified, such as the dispersive excitations which have minima at the incommensurate wavevectors $(0,0,1.875)$ and $(0,0,2.15)$ at $E = 1.9$ meV and overlap with m_2 at $(0,0,2)$. Finally above 3 meV broad diffuse scattering is observed due to the multi-particle continua and overlapping modes. The dispersions of the E_8 particles are expected to follow the theoretical expression given by Eq. (8), which can be modified as

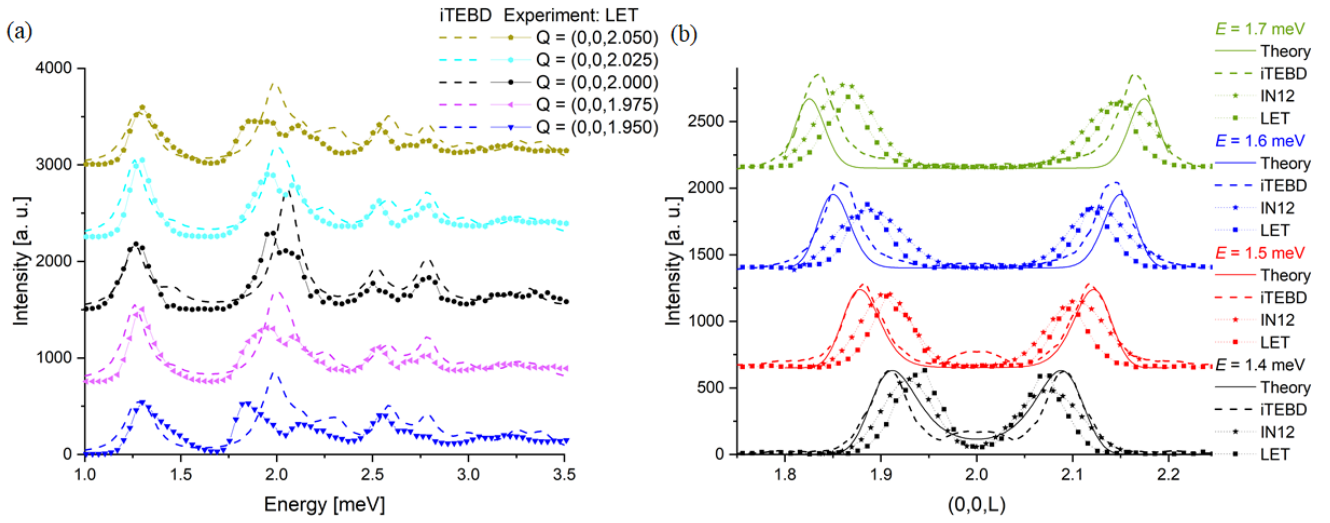


FIG. 4: (a) Comparison of DSF results between the iTEBD and the LET experimental data for constant momentum cuts. (b) Comparison of DSF results between the iTEBD data, the analytical data, and the experimental IN12 and LET data for constant energy cuts. The presented LET experimental constant momentum and constant energy cuts are shifted by an offset of 0.004 r.l.u (the offset was caused by experimental conditions). All DSF intensities are normalized up to the maximum intensity of experimental data.

$$E_i = \sqrt{\Delta_i^2 + (\gamma \cdot (L - 2))^2}, \quad (5)$$

where the single parameter $\gamma = \frac{\hbar\pi c}{2d}$ can be extracted. We simultaneously fit the lowest three E_8 dispersions and get the value $\gamma = 8.07$ meV. The fitted dispersions are given by the red lines in Fig. 3 (c) and show good agreement with the data. The ‘speed of light’ was extracted from γ and found to be $c \approx (1.643 \pm 0.041) \times 10^3$ m/s (using $d = 2.105$ Å - the projection of the nearest neighbor Co^{2+} - Co^{2+} distance onto the \mathbf{c} -axis). The value of γ , found from fitting the lowest three E_8 dispersions in the case of LET data, is $\gamma = 8.81$ meV and the ‘speed of light’ is found to be $c \approx (1.794 \pm 0.008) \times 10^3$ m/s. This value agrees well with the value of $c \approx (1.441 \pm 0.096) \times 10^3$ m/s found from iTEBD.

We further compare experimental, analytical, and numerical data with constant momentum scans [Fig. 4(a)] and constant energy scans [Fig. 4 (b)]. For the former comparison in Fig. 4(a) the analytical data are not included due to the presence of zone-folding effects for energies above 2 meV. The iTEBD data agree very well with the experimental data. For the latter comparison Fig. 4(b) in order to avoid mixture from zone-folding effect the energy window is chosen to match with the dispersion of the lightest E_8 particle. The analytical and iTEBD data show excellent agreement with each other, and both show good agreement with the experimental data. We note that there is about 1% deviation in momentum for the peak position corresponding to 1% m_1 energy shift. This possibly is because the transverse field, applied during the experiment, is slightly smaller than the exact critical field which can result in slightly heavier E_8 particles which implies a slightly

larger minimum gap m_1 . 1% m_1 shift corresponds to about 0.1 T to 0.2 T shift from the exact critical field whose value lies in the range of the identified putative QCP 4.7 ± 0.3 T [8].

To conclude, the quasi-1D antiferromagnet $\text{BaCo}_2\text{V}_2\text{O}_8$ is a very important material in the field of quantum magnetism. Among its unique properties are: Ising-like anisotropy, large intrachain versus weak but non-negligible interchain interactions, an anisotropic g tensor producing easy-axis anisotropy, and effective staggered fields under the application of an external magnetic field. Combining the results of INS experiments, theoretical, and numerical iTEBD simulations, we have precisely studied the E_8 excitation spectrum appearing at the one-dimensional quantum critical point of $B_c^{1D} = 4.7$ T. The observation of dynamical spectra through INS, together with excellent agreement with analytical analysis and iTEBD numerical simulations, enabled us to observe the dispersion of the first three E_8 particles and several multi-particles modes, paving the way toward possible manipulation of the E_8 particles.

The crystal growth and characterization took place at the Core Laboratory Quantum Materials, Helmholtz Zentrum Berlin für Materialien und Energie, Germany and at the Center for Advanced High Magnetic Field Science, Graduate School of Science, Osaka University. The authors would like to thank ISIS and ILL facilities for the allocation of neutron beamtime. We would like to also thank C. Fritsche for his help in the preparation of the sample holder. K. P. is also very grateful to Dr. C. Rohr for all his important suggestions about the general structure of the article. The LET data (<https://doi.org/10.5286/ISIS.E.RB2210086>) were reduced using Mantid and were analyzed using the Horace-MATLAB software package. This work has, in part, been supported by National Natural Science Foundation of China No.

U2032213 (J. M.), 12274288 (X. W. and J. W.) and the Innovation Program for Quantum Science and Technology Grant No. 2021ZD0301900 (X. W. and J. W.), 2022YFA1402702 (J. M.), and the Natural Science Foundation of Shanghai with grant No. 20ZR1428400 and Shanghai Pujiang Program with grant No. 20PJ1408100 (X.W. and J.W.), and Grants-in-Aid for Scientific Research (Nos. 25220803 and 24244059) from MEXT.

X. W. and K. P. contributed equally to this study. J. W., J. M., and B. L. conceived and coordinate the project. J. M., C. B, and B. L. designed the experiment. X. W. and J. W. carry out analytical and iTEBD calculations and provide theoretical analysis. X. W., K. P., J. M., J. W., and B. L. wrote the manuscript.

* jma3@sjtu.edu.cn

† wujd@sjtu.edu.cn

‡ bella.lake@helmholtz-berlin.de

- [1] S. Sachdev, *Quantum Phase Transitions* (Cambridge University Press, Cambridge, England, 2011) pp. 1–521.
- [2] A. B. Zamolodchikov, *Int. J. Mod. Phys. A* **4**, 4235 (1989).
- [3] P. Dorey, *Lect. Notes Phys.* **498**, 85 (1997).
- [4] H. Braden, E. Corrigan, P. Dorey, and R. Sasaki, *Nucl. Phys. B* **338**, 689 (1990).
- [5] P. Pfeuty, *Ann. Phys.* **59**, 79 (1970).
- [6] D. Boyanovsky, *Phys. Rev. B* **39**, 6744 (1989).
- [7] G. Delfino and G. Mussardo, *Nucl. Phys. B* **455**, 724 (1995).
- [8] H. Zou, Y. Cui, X. Wang, Z. Zhang, J. Yang, G. Xu, A. Okutani, M. Hagiwara, M. Matsuda, G. Wang, and et al., *Phys. Rev. Lett.* **127** (2021).
- [9] Z. Zhang, K. Amelin, X. Wang, H. Zou, J. Yang, U. Nagel, T. Röm, T. Dey, A. A. Nugroho, T. Lorenz, J. Wu, and Z. Wang, *Phys. Rev. B* **101**, 220411 (2020).
- [10] X. Wang, H. Zou, K. Hódsági, M. Kormos, G. Takács, and J. Wu, *Phys. Rev. B* **103**, 235117 (2021).
- [11] R. Coldea, D. A. Tennant, E. M. Wheeler, E. Wawrzynska, D. Prabhakaran, M. Telling, K. Habicht, P. Smeibidl, and K. Kiefer, *Science* **327**, 177–180 (2010).
- [12] C. M. Morris, N. Desai, J. Viirik, D. Hüvonen, U. Nagel, T. Röm, J. W. Krizan, R. J. Cava, T. M. McQueen, S. M. Koohpayeh, R. K. Kaul, and N. P. Armitage, *Nature Phys.* **17**, 832–836 (2021).
- [13] M. Fava, R. Coldea, and S. A. Parameswaran, *Proc. Nat. Acad. Sci.* **117**, 25219 (2020).
- [14] Q. Faure *et al.*, *Nature Phys.* **14**, 716 (2018).
- [15] S. K. Niesen, G. Kolland, M. Seher, O. Breunig, M. Valldor, M. Braden, B. Grenier, and T. Lorenz, *Phys. Rev. B* **87**, 224413 (2013).
- [16] E. Canévet, B. Grenier, M. Klanjšek, C. Berthier, M. Horvatić, V. Simonet, and P. Lejay, *Phys. Rev. B* **87**, 054408 (2013).
- [17] Y. Cui, H. Zou, N. Xi, Z. He, Y. X. Yang, L. Shu, G. H. Zhang, Z. Hu, T. Chen, R. Yu, J. Wu, and W. Yu, *Phys. Rev. Lett.* **123**, 067203 (2019).
- [18] G. Vidal, *Phys. Rev. Lett.* **98**, 070201 (2007).
- [19] B. Lake, K. Puzniak, J. Ma, and C. Balz, *Dispersion of E_8 particles in the spin-1/2 antiferromagnetic XXZ chain $BaCo_2V_2O_8$ in a transverse magnetic field*, *Ph.D. thesis* (2022).
- [20] S. Kimura, K. Okunishi, M. Hagiwara, K. Kindo, Z. He, T. Taniyama, M. Itoh, K. Koyama, and K. Watanabe, *J. Phys. Soc. Jpn.* **82**, 033706 (2013).
- [21] H. Zou, R. Yu, and J. Wu, *J. Phys.: Condens. Matt.* **32**, 045602 (2019).
- [22] J. Wu, M. Kormos, and Q. Si, *Phys. Rev. Lett.* **113**, 247201 (2014).
- [23] J. Yang, X. Wang, and J. Wu, *J. Phys. A: Math. Theor.* **56**, 013001 (2023).
- [24] M. Caselle and M. Hasenbusch, *Nucl. Phys. B* **579**, 667 (2000).
- [25] N. Hatano and M. Suzuki, *Quantum Annealing and Other Optimization Methods* (Springer Berlin Heidelberg, Berlin, Heidelberg, 2005) pp. 37–68.
- [26] I. Danshita and P. Naidon, *Phys. Rev. A* **79**, 043601 (2009).
- [27] D. Borthwick and S. Garibaldi, *Not. Amer. Math. Soc.* **58**, 1055 (2011).

Supplemental Material—Spin dynamics of the E_8 particles

Details of neutron experiments

Two large, high-quality single crystals of $\text{BaCo}_2\text{V}_2\text{O}_8$ were grown using the floating-zone technique at Osaka University, Japan, and at the Core Lab for Quantum Materials, Helmholtz Zentrum Berlin für Materialien und Energie (HZB), Germany. Inelastic neutron scattering was performed to measure the magnetic excitations on the cold neutron multichopper spectrometer, LET (at the ISIS Facility, Rutherford Appleton Laboratory, UK) using the HZB crystal (mass 4.13 g) [19]. INS experiments were also performed on the cold neutron triple-axis spectrometer, IN12 from the Forschungszentrum Jülich Collaborating Research Group (FZJ-CRG) installed at Institut Laue Langevin (ILL) France, using the Osaka crystal (mass 3.66 g).

For the LET experiment, the single crystal was aligned in the (0,K,L) horizontal scattering plane and a vertical field cryomagnet was used to apply a constant magnetic field of $B = 4.7$ T along the \mathbf{a} -axis to reach the 1D QCP. These measurements were carried out at $T = 0.3$ K using a ^3He -insert. This temperature is well below the Néel temperature ($T_N = 5.5$ K) ensuring the presence of the effective longitudinal perturbing field necessary to stabilize E_8 physics. Using repetition rate multiplication and the chopper frequencies 280/140 Hz, incident neutron energies of $E_i = 22.69, 13.21, 8.51, 6.00, 4.42, 3.42, 2.70$ meV were achieved with corresponding elastic energy resolutions of $\Delta E = 0.91, 0.41, 0.22, 0.14, 0.094, 0.065, 0.048$ meV. The INS data were processed using the MANTID and HORACE software packages and converted to absolute units.

For the IN12 experiment, the crystal was aligned with the \mathbf{a} - and \mathbf{c} -axes within the horizontal instrumental scattering plane and a vertical DC magnetic field of 4.7 T was applied parallel to the \mathbf{b} -axis. A fixed final wavevector of $k_f = 1.15 \text{ \AA}^{-1}$ was used, giving an energy resolution of $\Delta E \approx 0.114$ meV and wavevector resolution of ≈ 0.067 r.l.u. A Beryllium filter was used to suppress higher-order wavelengths and spurious scattering.

Theoretical model and dispersion of E_8 particles

When applying a transverse field along (0,1,0) direction, the effective Hamiltonian for $\text{BaCo}_2\text{V}_2\text{O}_8$ is described by a 1D spin-1/2 Heisenberg-Ising model [8, 17, 20, 21]:

$$\begin{aligned}
 \mathcal{H} &= H_{XZX} + H_t + H_s \\
 H_{XZX} &= J \sum_n [S_n^z S_{n+1}^z + \epsilon (S_n^x S_{n+1}^x + S_n^y S_{n+1}^y)] \\
 H_t &= -\mu_B g_{yy} H \sum_n [S_n^y + h_x (-1)^n S_n^x \\
 &\quad + h_z \cos(\pi \frac{2n-1}{4}) S_n^z] \\
 H_s &= -\mu_B H' \sum_n (-1)^n S_n^z
 \end{aligned} \tag{6}$$

where $S_n^\alpha = \frac{1}{2} \sigma_n^\alpha$ ($\alpha = x, y, z$) are spin-1/2 operators at site n with Pauli matrices σ^α . $J = 5.8$ meV, $\epsilon = 0.46$, $h_{x(z)} = 0.4(0.14)$, $g_{yy} = 2.75$. The applied transverse field is set $\mu_0 H = 4.7$ T, which is the critical field of the putative 1D QCP [8, 21]. The effective staggered longitudinal field $\mu_B H' = 0.018J$ comes from a mean-field treatment of the inter-chain coupling in the 3D ordering region below T_N [8, 14]. H_s provides a necessary relevant perturbation for realizing the quantum E_8 physics [8]. Focusing on the parameter region around the putative 1D QCP, in the scaling limit, the effective Hamiltonian of the spin chain becomes [7, 8, 10]

$$\mathcal{H}_{E_8} = \mathcal{H}_{c=1/2} + h \int dx \sigma(x). \tag{7}$$

$\mathcal{H}_{c=1/2}$ is the Hamiltonian for a central charge 1/2 conformal field theory, which describes the quantum critical physics of the TFIC. h and $\sigma(x)$ corresponding to the scaling limits of $\mu_B H'$ and σ_j^z are the strengths of the perturbation field and the relevant primary field, respectively. To determine the dispersion of E_8 particles and compare with the spectrum measured by INS, we calculate the DSF in the field theory frame, $D^{\alpha\alpha}(\omega, q) = \sum_{n=1}^{\infty} \frac{(2\pi)^2}{\prod_{a_i=1}^8 n_{a_i}!} \int_{-\infty}^{\infty} \prod_{j=1}^n \frac{d\theta_j}{2\pi} |\langle 0 | \sigma^\alpha | A_{a_1}(\theta_1) \dots A_{a_n}(\theta_n) \rangle|^2 \delta(\omega - \sum_{j=1}^n E_j) \delta(q - \sum_{j=1}^n P_j)$, where $\alpha = x, z$, and $a_i = 1 \dots 8$ are quasi-particles obtained from the quantum E_8 integrable theory [2, 7, 8, 10]. n_{a_i} is the number of particle a_i involved in the corresponding channel. $E_j = m_{a_j} \cosh \theta_j$ and $P_j = m_{a_j} \sinh \theta_j$ are the energy and momentum of particle a_j in terms of the rapidity θ , respectively. The two Dirac δ -functions reflect the energy and momentum conservation of the scattering. The DSF of $\sigma^{x,z}$ can be directly calculated from quantum E_8

integrable field theory [10], and the DSF of σ^y can be obtained from DSF of σ^z [22]. For a better comparison of the theoretical prediction from quantum E_8 field theory with the INS experimental result, two subtle issues are worth noting.

1. In the above field theory frame calculation, the speed of light is set as $c = 1$. For the quantum E_8 model, as a massive relativistic quantum field theory, the dispersion of the E_8 particles follows the massive relativistic dispersion $E_i^2 = \Delta_i^2 + p_i^2 c^2$, where $\Delta_i = m_i c^2$ and $p_i = m_i c$ with the “rest mass” of the i^{th} E_8 particle m_i and the “speed of light” c . When coming to a real material which actually is a lattice discrete in space, we need to re-scale the dispersion of the E_8 particles with the proper energy scale and length (momentum) scale serving as IR cutoffs. The theoretically expected energy peak corresponding to the lightest E_8 particle m_1 can be estimated from $E_{m_1}^{\text{theory}} = C_{\text{lattice}} H^{18/15} \approx 1.2 \text{ meV}$ [23], where $C_{\text{lattice}} = 4.010 \dots$ is a modified constant for the lattice which originally comes from quantum E_8 field theory [24]. The value of $E_{m_1}^{\text{iTEBD}}$ matches the minimum gap $\Delta_1 = 1.26 \text{ meV}$ observed at the zone center (corresponding to zero transfer momentum), thus Δ_1 can naturally serve as IR cutoff of the energy scale for the experimental data. Since $\Delta_1 = m_1 c^2$ then we can pick up the corresponding IR momentum cutoff $p_1 = m_1 c$. By applying these two IR cutoffs scales we arrive at

$$\frac{E_i^2}{\Delta_1^2} = \frac{\Delta_i^2}{\Delta_1^2} + \frac{p_i^2}{(\Delta_1/c)^2} = \frac{\Delta_i^2}{\Delta_1^2} + \left(\frac{\hbar(L-2)\pi/2d}{m_1 c} \right)^2, \quad (8)$$

where $p_i = \hbar(L-2)\pi/2d$ is the momentum transfer with respect to $\mathbf{Q} = (0,0,2)$ and $d = 8.4192/4 = 2.105$ is the nearest neighbor distance between Co^{2+} ions projected onto the chain direction. We need to determine the value of c to obtain the IR cutoff for the momentum, whose value cannot be uniquely determined by the analytical theory but actually depends on the microscopic details of the material.

2. The four-fold periodicity of $\text{BaCo}_2\text{V}_2\text{O}_8$ leads to the sizable zone-folding effect of the experimental measurement, which makes the E_8 particles’ dispersion shadowed by additional spectra. Such an effect cannot be obtained from the field theory calculation, instead, we need to go back to the original effective lattice model. By comparing spectra obtained from the lattice model and the field theory, the E_8 particles’ dispersion will be extracted. To make these two subtle issues clear, we carry out iTEBD simulation for the effective Hamiltonian Eq. (6) with $J = 1$, $\epsilon = 0.47$, and critical field $\mu_B g_{yy} H = 0.15$ [8, 21],

$$D_{\text{lat}}^{\alpha\alpha}(\omega, q) = \frac{1}{N} \sum_{j,j'=1}^N \exp\{-iq(j-j')\} \times \int_{-\infty}^{\infty} dt \exp(i\omega t) \langle S_j^\alpha(t) S_{j'}^\alpha(0) \rangle, \quad (9)$$

with total number of lattice sites N ($N \rightarrow \infty$ in iTEBD), and spin-1/2 operators S^α , $\alpha = x, y, z$. The procedure of the iTEBD calculation is as follows: 1. Generate a four-periodic ground state wave function of the effective Hamiltonian Eq. (6) with the parameters. The imaginary time-evolution is done with fifth-order Trotter-Suzuki decomposition [25], where the imaginary time slide is set as $d\tau = 0.01$. The convergence condition is chosen as the difference of the norm of singular values in the matrix product states being smaller than 10^{-12} . The truncated dimension is chosen as $\chi = 45$ [18, 26]. 2. Calculate the DSF [Eq. (9)] for S^x and S^z , while the DSF of S^y can be obtained from DSF of S^z by using $D^{yy}(\omega, q) = \omega^2 D^{zz}(\omega, q)/(4J^2)$ [22]. For calculating this DSF with iTEBD algorithm, we first do real time and space propagation in Heisenberg picture, then by using Fourier transformation we transform the obtained result into momentum and energy space to obtain the final spectrum. The real time evolution is done by a second order Trotter-Suzuki decomposition with $t = 200$, $dt = 0.02$ for obtaining a relatively high accurate result near the Brillouin zone center. 3. A zone-folding effect is necessary to consider when obtaining the final spectrum for comparison with INS experimental results.

* jma3@sjtu.edu.cn

† wujd@sjtu.edu.cn

‡ bella.lake@helmholtz-berlin.de

- [1] S. Sachdev, *Quantum Phase Transitions* (Cambridge University Press, Cambridge, England, 2011) pp. 1–521.
[2] A. B. Zamolodchikov, *Int. J. Mod. Phys. A* **4**, 4235 (1989).
[3] P. Dorey, *Lect. Notes Phys.* **498**, 85 (1997).
[4] H. Braden, E. Corrigan, P. Dorey, and R. Sasaki, *Nucl. Phys. B* **338**, 689 (1990).
[5] P. Pfeuty, *Ann. Phys.* **59**, 79 (1970).
[6] D. Boyanovsky, *Phys. Rev. B* **39**, 6744 (1989).
[7] G. Delfino and G. Mussardo, *Nucl. Phys. B* **455**, 724 (1995).

- [8] H. Zou, Y. Cui, X. Wang, Z. Zhang, J. Yang, G. Xu, A. Okutani, M. Hagiwara, M. Matsuda, G. Wang, and et al., *Phys. Rev. Lett.* **127** (2021).
- [9] Z. Zhang, K. Amelin, X. Wang, H. Zou, J. Yang, U. Nagel, T. Rõ om, T. Dey, A. A. Nugroho, T. Lorenz, J. Wu, and Z. Wang, *Phys. Rev. B* **101**, 220411 (2020).
- [10] X. Wang, H. Zou, K. Hódsági, M. Kormos, G. Takács, and J. Wu, *Phys. Rev. B* **103**, 235117 (2021).
- [11] R. Coldea, D. A. Tennant, E. M. Wheeler, E. Wawrzynska, D. Prabhakaran, M. Telling, K. Habicht, P. Smeibidl, and K. Kiefer, *Science* **327**, 177–180 (2010).
- [12] C. M. Morris, N. Desai, J. Viirok, D. Hüvonen, U. Nagel, T. Rõ om, J. W. Krizan, R. J. Cava, T. M. McQueen, S. M. Koohpayeh, R. K. Kaul, and N. P. Armitage, *Nature Phys.* **17**, 832–836 (2021).
- [13] M. Fava, R. Coldea, and S. A. Parameswaran, *Proc. Nat. Acad. Sci.* **117**, 25219 (2020).
- [14] Q. Faure *et al.*, *Nature Phys.* **14**, 716 (2018).
- [15] S. K. Niesen, G. Kolland, M. Seher, O. Breunig, M. Valldor, M. Braden, B. Grenier, and T. Lorenz, *Phys. Rev. B* **87**, 224413 (2013).
- [16] E. Canévet, B. Grenier, M. Klanjšek, C. Berthier, M. Horvatić, V. Simonet, and P. Lejay, *Phys. Rev. B* **87**, 054408 (2013).
- [17] Y. Cui, H. Zou, N. Xi, Z. He, Y. X. Yang, L. Shu, G. H. Zhang, Z. Hu, T. Chen, R. Yu, J. Wu, and W. Yu, *Phys. Rev. Lett.* **123**, 067203 (2019).
- [18] G. Vidal, *Phys. Rev. Lett.* **98**, 070201 (2007).
- [19] B. Lake, K. Puzniak, J. Ma, and C. Balz, *Dispersion of E_s particles in the spin-1/2 antiferromagnetic XXZ chain $BaCo_2V_2O_8$ in a transverse magnetic field*, *Ph.D. thesis* (2022).
- [20] S. Kimura, K. Okunishi, M. Hagiwara, K. Kindo, Z. He, T. Taniyama, M. Itoh, K. Koyama, and K. Watanabe, *J. Phys. Soc. Jpn.* **82**, 033706 (2013).
- [21] H. Zou, R. Yu, and J. Wu, *J. Phys.: Condens. Matt.* **32**, 045602 (2019).
- [22] J. Wu, M. Kormos, and Q. Si, *Phys. Rev. Lett.* **113**, 247201 (2014).
- [23] J. Yang, X. Wang, and J. Wu, *J. Phys. A: Math. Theor.* **56**, 013001 (2023).
- [24] M. Caselle and M. Hasenbusch, *Nucl. Phys. B* **579**, 667 (2000).
- [25] N. Hatano and M. Suzuki, *Quantum Annealing and Other Optimization Methods* (Springer Berlin Heidelberg, Berlin, Heidelberg, 2005) pp. 37–68.
- [26] I. Danshita and P. Naidon, *Phys. Rev. A* **79**, 043601 (2009).
- [27] D. Borthwick and S. Garibaldi, *Not. Amer. Math. Soc.* **58**, 1055 (2011).